PHYSICAL REVIEW B **89**, 174519 (2014)

Evolution of London penetration depth with scattering in single crystals of $K_{1-x}Na_xFe_2As_2$

H. Kim,[1,2] M. A. Tanatar,[1,2] Yong Liu,[1] Zachary Cole Sims,[3] Chenglin Zhang,[3,4] Pengcheng Dai,[4] T. A. Lograsso,[1] and R. Prozorov[1,2,*]

[1]*Ames Laboratory, Ames, Iowa 50010, USA*

[2]*Department of Physics & Astronomy, Iowa State University, Ames, Iowa 50010, USA*

[3]*Department of Physics and Astronomy, The University of Tennessee, Knoxville, Tennessee 37996-1200, USA*

[4]*Department of Physics and Astronomy, Rice University, Houston, Texas 77005, USA*

(Received 24 March 2014; revised manuscript received 16 May 2014; published 30 May 2014)

London penetration depth, $\lambda(T)$, was measured in single crystals of $K_{1-x}Na_xFe_2As_2$, $x = 0$ and 0.07, down to temperatures of 50 mK, $\sim T_c/50$. Isovalent substitution of Na for K significantly increases impurity scattering, with $\rho(T_c)$ rising from 0.2 to 2.2 $\mu\Omega$ cm, and leads to a suppression of T_c from 3.5 to 2.8 K. At the same time, a close to T-linear $\Delta\lambda(T)$ in pure samples changes to almost T^2 in the substituted samples. The behavior never becomes exponential as expected for the accidental nodes, as opposed to T^2 dependence in superconductors with symmetry imposed line nodes. The superfluid density in the full temperature range follows a simple clean and dirty d-wave dependence, for pure and substituted samples, respectively. This result contradicts suggestions of multiband scenarios with strongly different gap structure on four sheets of the Fermi surface.

DOI: 10.1103/PhysRevB.89.174519 PACS number(s): 74.70.Xa, 74.20.Rp, 74.25.Ha

I. INTRODUCTION

The discussion of the superconducting pairing mechanism in iron-based superconductors was guided by early observations of a full superconducting gap in tunneling experiments [1], which was seemingly at odds with the neutron resonance peak [2], suggesting a sign change of the order parameter. Theoretically, Mazin *et al.* suggested a pairing mechanism, in which the superconducting order parameter changes sign between hole and electron bands, but each band remains fully gapped [3,4]. Verification of this so-called $s_\pm$ pairing quickly became a focal point of studies of the superconducting gap structure.

Clear deviations from the full-gap $s_\pm$ pairing scenario were found in nuclear magnetic resonance (NMR) and heat capacity studies of KFe_2As_2 (K122) [5], which represents the terminal overdoped composition of the $Ba_{1-x}K_xFe_2As_2$ series (BaK122) [6,7]. Systematic doping evolution studies over the whole superconducting dome in $Ba(Fe_{1-x}Co_x)_2As_2$ (BaCo122) [8–14], $NaFe_{1-x}Co_xAs$ [15,16], and $Ba_{1-x}K_xFe_2As_2$ [17] suggest that the superconducting gap in all cases mentioned above develops evident anisotropy and even nodes at the dome edges. Thus K122 is not unique as a nodal superconductor. On the other hand, it is one of the cleanest stoichiometric materials and, therefore, understanding its superconducting gap is of great importance for the entire iron-based family.

Such diverse evolution of the superconducting gap with doping in iron-based superconductors is notably different from the cuprates, in which nodal d-wave pairing is observed in all doping regimes and families of materials. Several theoretical explanations of this fact were suggested [18–20]. The observed doping evolution was explained in $s_\pm$ pairing scenario as a result of the competition between interband pairing and intraband Coulomb repulsion [19,21]. Alternatively, it was explained to be due to a phase transition between $s_\pm$-wave and d-wave superconducting states [18]. The important difference is that the nodes in the gap structure are accidental in the former scenario but are symmetry-imposed in the latter.

The existence of line nodes in the superconducting gap of K122 is supported by experiments. London penetration-depth studies found close to T-linear temperature dependence [22]. The analysis of vortex lattice symmetry in small-angle neutron scattering suggested horizontal line nodes in the gap [23]. Thermal conductivity studies revealed robust finite residual linear term in zero field, which rapidly increases with magnetic field [24,25]. Moreover, the residual linear term was found to be independent of the heat flow direction [25] and impurity scattering [25,26], suggesting the presence of symmetry-imposed vertical line nodes in the superconducting gap, similar to the d-wave superconducting state of the cuprates [27]. Measurements of the specific heat in Na-doped samples are consistent with a d-wave pairing [28,29]. Moreover, nonmonotonic dependence of T_c on pressure was explained as evidence of a phase transition from d-wave to s-wave symmetry in the superconducting state of K122 [30,31].

However, these observations consistent with d-wave scenario are disputed by laser angle-resolved photoemission spectroscopy (ARPES) [32], suggesting an extreme multiband scenario in which the all line nodes are observed only on one hole band (octuplet node scenario), with three other sheets being fully gapped. Two recent heat capacity studies [33,34] observed a clear feature at around 0.7 K, with the general view of the curves very similar to the multiband MgB_2 [35]. Hardy *et al.* [33] pointed out the importance of measurements with temperatures below 100 mK and were able to fit an experimental C_e/T curve in the whole superconducting region, including the feature at 0.7 K, assuming four full-gap contributions, three of which have anomalously small gaps (lilliputian gap scenario). It is important to notice though that both ARPES and heat capacity measurements probe changes induced by opening of the superconducting gap in the normal state, not of the condensate itself. The former is in addition probing the states at the top layer of the sample surface, prone

*Corresponding author: prozorov@ameslab.gov

to modification by surface reconstruction [36]. Heat capacity measurement is a bulk probe, but by nonselective probing the whole sample can be affected by the presence of impurity phases. The admixture of the magnetic impurity phases was invoked for the explanation of 0.7 K features in other heat capacity studies [37,38].

In this paper we report systematic studies of the London penetration depth in pure KFe_2As_2 and isovalently substituted $K_{1-x}Na_xFe_2As_2$ (KNa122). We show that the temperature-dependent superfluid density calculated with experimental London penetration depth and its response to the pair-breaking due to non-magnetic scattering are consistent with the symmetry-imposed line nodes in the superconducting gap, in contrast to the extreme multiband scenario.

II. EXPERIMENT

Single crystals of KFe_2As_2 were grown using the KAs flux method as explained in Ref. [39]. Single crystals of $K_{1-x}Na_xFe_2As_2$ were grown by mixing (NaK)As/FeAs in sealed tantalum tubes, followed by cooking at 1150 °C for 3 hours and 5 °C/h cooling down to room temperature [40]. The wavelength dispersive x-ray spectroscopy (WDS) in a JEOL JXA-8200 electron microprobe was utilized to determine the chemical compositions. The actual concentration x was determined by averaging results of 12 measurements on different locations per single crystal, statistical error of the composition is ± 0.005. Small resistance contacts ($\sim 10\mu\Omega$) were tin-soldered [41,42], and in-plane resistivity was measured using a four probe technique in a Quantum Design physical property measurement system (PPMS). The London penetration depth was measured in samples with typical dimensions of $0.8 \times 0.8 \times 0.1$ mm^3 by using a tunnel diode resonator (TDR) technique [43] in a ^{3}He cryostat and a dilution refrigerator with operation frequencies of $f_0 =$ 14 MHz and 17 MHz, respectively. The ^{3}He-TDR was used for measurements down to $T = 0.5$ K, and the measurements were extended to lower temperatures down to $T = 0.05$ K by using the dilution refrigerator-TDR. The samples were inserted into a 2 mm inner diameter copper coil that produces an rf excitation field with amplitude $H_{ac} \sim 20$ mOe, which is much smaller than a typical first critical field. Measurements of the in-plane penetration depth, $\Delta\lambda(T)$, were done with $H_{ac} \parallel c$ axis. The shift of the resonant frequency is related to magnetic susceptibility of the specimen via $\Delta f(T) = -G4\pi\chi(T)$ (in cgs units) where $\chi(T)$ is the differential magnetic susceptibility, $G = f_0 V_s/2V_c(1-N)$ is a constant, N is the demagnetization factor, V_s is the sample volume, and V_c is the coil volume. The constant G was determined from the full frequency change by physically removing the sample out of the coil. With the characteristic sample size R, which can be calculated by the procedure explained in Ref. [44], $4\pi\chi = (\lambda/R)\tanh(R/\lambda) - 1$, from which $\Delta\lambda$ can be obtained [44,45]. The frequency shift measured with the TDR technique in the normal state represents skin depth δ, provided that dimensions of the sample are much greater than δ and are due to the normal skin effect [46,47]. This measured skin depth can be converted into the resistivity ρ by using the relation $\delta = c/(2\pi\sqrt{\rho/f_0})$ (cgs units), where c is the speed of light.

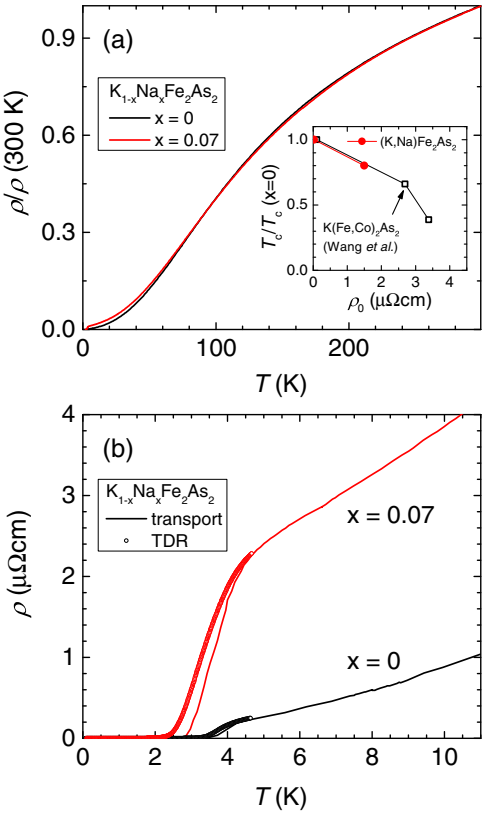

FIG. 1. (Color online) (a) In-plane electrical resistivity of $K_{1-x}Na_xFe_2As_2$ with $x = 0$ and $x = 0.07$ shown over the full temperature range using the normalized resistivity scale $\rho(T)/\rho(300\text{ K})$ and (b) zoomed on the superconducting transition region (lines) using the actual ρ scale. Data points in panel (b) show temperature-dependent resistivity as determined from radio frequency skin-depth measurements in our TDR setup. The inset in panel (a) shows superconducting T_c, determined using the zero-resistance criterion, as a function of the residual resistivity estimated from the Fermi-liquid fit, $\rho = \rho_0 + AT^2$ in isovalent-substituted $K_{1-x}Na_xFe_2As_2$ (circles) in comparison with the electron-doped $K(Fe_{1-x}Co_x)_2As_2$ (squares) obtained by Wang *et al.* [26].

III. RESULTS AND DISCUSSION

Panel (a) of Fig. 1 shows temperature-dependent resistivity of $K_{1-x}Na_xFe_2As_2$ with $x = 0$ and 0.07 using the normalized resistivity scale $\rho/\rho(300\text{ K})$. The zoom on the superconducting transition in panel (b) shows the same data in actual resistivity values. Because of the significant scatter in the resistivity values in iron-based superconductors due to the presence of hidden cracks [48,49], we used statistically significant $\rho(300\text{ K}) = 285 \pm 50\ \mu\Omega\,\text{cm}$ (as determined in Ref. [50] by the average and standard deviation of measurements on 12 crystals) for pure samples. The values at the lower boundary of the error bars provided the best agreement with TDR skin depth measurements, due to being less prone to cracks [51]. Within rather big error bars of the resistivity measurements, the resistivity value for Na-doped samples is indistinguishable from that of the pure material at high temperatures, so we adopted the same $\rho(300\text{ K})$. The $\rho(T)$ of two sets of samples are identical as well, except for the increased residual resistivity and suppression of the

superconducting transition temperature in $x = 0.07$ samples. The actually measured values of resistivity before the first signatures of superconductivity are 0.2 and 2.2 $\mu\Omega$ cm. Because of the strong temperature dependence of resistivity before onset of the superconducting transition, these values are significantly larger than the extrapolated $T = 0$ residual resistivities of $0.100 \pm 0.050 (x = 0)$ and 1.7 $\mu\Omega$ cm ($x = 0.07$). The skin depths measured by the TDR technique show good agreement with the direct transport measurements as shown in Fig. 1(b).

Scattering introduced by Na substitution in $K_{1-x}Na_xFe_2As_2$ is clearly nonmagnetic; however, it provides strong pair breaking, as expected in unconventional superconductors, and substantially suppresses T_c. The inset in Fig. 1(a) shows T_c, as determined using the $\rho = 0$ criterion, as a function of ρ_0. For the reference we show similar data obtained in samples with aliovalent Co substitution in $K(Fe_{1-x}Co_x)_2As_2$ [26]. Despite the fact that Co substitution provides electron doping while Na substitution is isoelectronic, both types of substitution introduce similar pair-breaking, suggestive that scattering rather than electron count plays a primary role in T_c suppression.

The temperature-variation of the London penetration depth provides information about the structure of the superconducting gap. This statement is valid in a characteristic temperature range for which the superconducting gap $\Delta(T)$ can be considered constant. For single-gap superconductors the upper limit is approximately $T_c/3$. Below this temperature, $\Delta\lambda(T)$ shows exponential saturation in single-gap s-wave superconductors. In the multiband situation, however, the smallest gap determines the region of exponential behavior, and it can be much smaller than $T_c/3$. This is demonstrated in Fig. 2(a) for $K_{0.35}Ba_{0.65}Fe_2As_2$ [52], where the "upper low-temperature range" extends only up to $T_c/6$. Therefore, lowest temperature experiments are needed to probe multiband superconductivity.

For the gap with symmetry-imposed line nodes, $\Delta\lambda$ can be described by the power law $\Delta\lambda(T) = AT^n$, where the exponent n depends on impurity scattering and symmetry of the order parameter. For line nodes, the exponent n *increases* from the value of $n = 1$ in the clean limit to $n = 2$ in the dirty limit [53]. In $s_\pm$ pairing, however, the exponential dependence is expected for a clean case. Experimentally the data are still analyzed in terms of the power law, and for n greater than 3 it is difficult to distinguish from the exponential with realistic noise of the data points. Adding scattering in the $s_\pm$ pairing case, the exponent n *decreases* from a larger value to the same dirty limit value of $n = 2$ [54]. However, in the case of $s_\pm$ pairing with accidental nodes, disorder will lift the nodes, resulting in a change of the exponent n from 1 to exponential [55].

In Fig. 2(a) we show $\Delta\lambda$ versus $t = T/T_c$ of KNa122 crystals with $x = 0$ and $x = 0.07$. The inset shows the same data plotted as $\Delta\lambda$ versus t^2. It is clear that the exponent n *increases* with doping and, in the $x = 0.07$ sample, approaches the dirty-limit value $n = 2$. Both features are consistent with the superconducting gap with the symmetry-imposed line nodes. Specifically, the data between the base temperature of 50 mK and $T = T_c/3$ can be best fitted to the power-law function with $n = 1.39$, $A = 200$ nm and $n = 1.93$, $A = 911$ nm for $x = 0$ and 0.07, respectively. Both are in the range

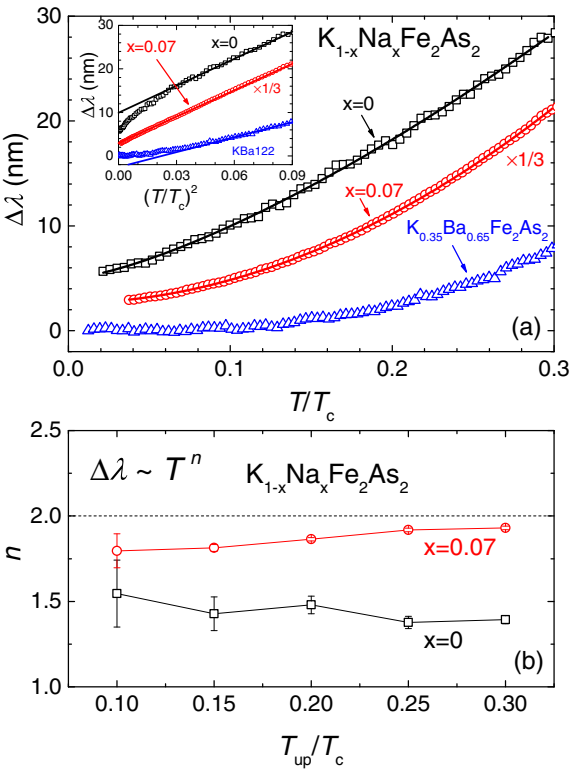

FIG. 2. (Color online) (a) Low temperature ($T \leqslant 0.3T_c$) variation of the London penetration depth in $K_{1-x}Na_xFe_2As_2$, $x = 0$ and $x = 0.07$, compared with a full-gap superconductor $K_{0.35}Ba_{0.65}Fe_2As_2$ [52]. The inset shows the same data plotted versus $(T/T_c)^2$ to highlight a subquadratic behavior of $\lambda(T)$ in clean samples and almost perfect T^2 dependence in Na-substituted samples. Data for $K_{1-x}Na_xFe_2As_2$ $x = 0$ and $x = 0.07$ are vertically shifted for clarity by 6 and 3 nm, respectively. The bottom panel (b) shows the exponent n in the power-law fits of the data, $\Delta\lambda(T) = AT^n$, plotted versus the upper limit of the fitting range from the base temperature, $T_{min} = 50$ mK to T_{up}. Note that neither $\Delta\lambda(T)$ raw data of panel (a) nor $n(T_{up})$ show any irregularities over the whole range (up to 1 K), the range where significant anomalies are observed in the specific heat data at and below 0.5–0.8 K [33,34].

expected for symmetry-imposed line nodes. According to Hirschfeld-Goldenfeld's theory [53], the penetration depth can be interpolated as $\Delta\lambda(T) = \lambda(0)T^2/(T + T^*)$ where T^* is a crossover temperature from T to T^2 behavior at the low temperatures. Our fit in pure K122 using this formula gives $T^* = 0.5T_c$. On the other hand, this expression is inapplicable for the Na-substituted sample that shows quadratic behavior at all temperatures, indicating that these samples are in the dirty limit.

Alternatively, as discussed above, this crossover behavior can be due to the multiband effects in superconductivity. For multiband superconductors the upper end of the characteristic $\Delta\lambda(T)$ dependence is determined by the smaller gap Δ_{min}, and shrinks proportionally to Δ_{min}/Δ. Since gap structure is not known, the upper limit of the characteristic behavior cannot be assumed *a priori*. Therefore, for quantitative analysis of the data we performed power-law fitting over the variable temperature interval. The low-temperature end of this interval was always kept fixed at the base temperature of about 50 mK, and the exponent of the power-law fit n was determined as a

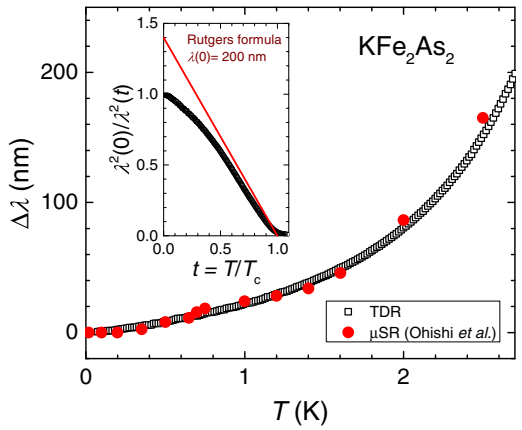

FIG. 3. (Color online) Variation of the London penetration depth in pure KFe_2As_2 (black squares) compared to the results from muon spin rotation experiments (red circles) by Ohishi *et al.* [56]. The μSR data provide a zero-temperature value of $\lambda(0) = 200$ nm, which we use to calculate the superfluid density $\rho_s(T)$, as shown in the inset. The line in the inset shows a slope of the $\rho_s(T)$ curve at T_c calculated using the thermodynamic Rutgers relation [57] from the specific heat jump and the slope of $H_{c2}(T)$ at T_c.

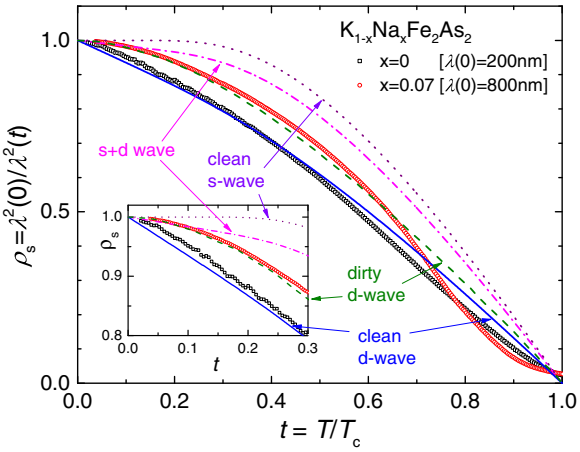

FIG. 4. (Color online) Superfluid density for $K_{1-x}Na_xFe_2As_2$ $x = 0$ and $x = 0.07$ compared with the theoretical predictions for different models of the superconducting gap structure. We include the single-band clean limit s-wave (dotted line) and d-wave (full line) cases, as well as dirty limit d-wave (dashed line). We also show superfluid density for the multiband scenario with nodes only on some of the bands (shown as "$s + d$" by a dot-dashed line), calculated using parameters of the Fermi surface and a combination of nodal and nodeless gaps as suggested by Okazaki *et al.* [32]. The data for the pure compound follow closely a clean limit d-wave curve, whereas the $\rho_s(T)$ for sample $x = 0.07$ follow the dirty d-wave dependence in a substantial portion of the full temperature range. The inset zooms at the low-temperature part, highlighting the differences in behavior.

function of the high-temperature end, T_{up}. This dependence of $n(T_{up})$ for KNa122 samples with $x = 0$ and $x = 0.07$ is shown in Fig. 2(b). Note that neither raw $\Delta\lambda(T)$ data of Fig. 2(a), nor $n(T_{up})$ of Fig. 2(b), show any irregularities over the range $t \leqslant 0.3$, which is consistent with other penetration depth measurements [22,56]. But this is in stark contrast with two reports of significant anomalies at about 0.7 K and below in the temperature-dependent specific heat [33,34].

A further insight into the structure of the superconducting gap in KFe_2As_2 can be obtained through the analysis of the temperature-dependent superfluid density, $\rho_s(T) = \lambda^2(0)/\lambda^2(T)$, with $\lambda(T) = \lambda(0) + \Delta\lambda(T)$. This quantity can be calculated for known superconducting gap structure and compared with the experiment over the full superconducting temperature range. To perform this analysis knowledge of $\lambda(0)$ is required, which is not readily available from our experiments. We used the value of $\lambda(0) = 200$ nm based on recent muon spin relaxation (μSR) experimental results [56] as well as experimental plasma frequencies [22], and we verify its consistency by using the thermodynamic Rutgers formula [57]. We note that 200 nm is the typical value for iron-based superconductors away from the coexistence-with-magnetism regime [11,58,59].

The main panel of Fig. 3 compares our TDR data (black squares) with μSR data (red dots) showing excellent agreement. The inset shows superfluid density calculated using $\lambda(0) = 200$ nm and comparison with the expected slope, calculated using the thermodynamic Rutgers formula [57] that connects the slope of $\rho_s(T)$ at T_c, $\rho_s' \equiv \frac{d\rho_s}{dT}$, with the slope of the $H_{c2}(T)$ at T_c, $H_{c2}' \equiv \frac{dH_{c2}}{dT}$, and the magnitude of the specific heat jump ΔC at T_c via

$$\frac{\rho_s'(T_c)}{\lambda^2(0)} = \frac{16\pi^2 T_c \Delta C}{\phi_0 H_{c2}'(T_c)}, \qquad (1)$$

where ϕ_0 is magnetic flux quantum. Taking the slope $H_{c2}' = -0.55$ T/K [60] and specific heat jump as $\Delta C =$ 159.6 mJ/mol K [60], we obtain the slope $\rho_s' = -1.4$ as shown in the inset in Fig. 3. It can be seen that the value of $\lambda(0) = 200$ nm is quite reasonable. For the sample with $x = 0.07$ we estimated $\lambda(0) = 0.8$ μm using Homes scaling based on the resistivity and T_c data [61,62]. The resulting $\rho_s(T)$ for both pure and $x = 0.07$ samples are shown in Fig. 4. The low-temperature parts of $\rho_s(T)$ are zoomed in the inset of Fig. 4. For comparison, Fig. 4 shows the expected temperature-dependent superfluid density in clean (full line) and dirty (dashed line) d-wave cases, which are representative of all superconductors with symmetry-imposed line nodes. Clearly, in a large portion of the full temperature range, the data for pure K122 follow a simple d-wave behavior, whereas the Na-substituted sample follows expectations for a dirty d-wave superconductor.

Since the multiband scenario is clearly suggested by both ARPES [32] and heat capacity studies [33,34], we now turn to a more realistic band/superconducting gap structure. Here we try to estimate the temperature-dependent superfluid density from the published band-structure, ARPES, quantum oscillations, and specific heat data, and we compare it with the experimental results. Three hole-like sheets of the Fermi surface centered around the Γ point will be considered. ARPES measurements concluded that there are two full, somewhat anisotropic gaps on the inner, α (Δ/k_BT_c varies between 2.7 and 5), and the outer, β (Δ/k_BT_c varies between 0.4 and 0.6), sheets and a nodal gap on the middle (ζ) sheet (Δ/k_BT_c varies between 0 and 2.6) [32]. In sharp contrast, the gap amplitudes from the fit of the specific heat are 0.57, 0.22, 0.35, and the surprisingly large value 1.90 on the electron-like ϵ Fermi sheet near the X points [33].

In a multiband system different sheets of the Fermi surface contribute partial superfluid densities as

$$\rho(t) = \sum \gamma_i \rho_i(t)$$

where the sum is over all contributing sheets, and

$$\gamma_i = \frac{n_i v_i^2}{\sum n_i v_i^2},$$

where

$$n_i = \frac{N_i(0)}{N(0)} = \frac{N_i(0)}{\sum N_i(0)}$$

is the normalized total density of states at each band for both spin directions and v_i is the Fermi velocity. To evaluate superfluid density and to estimate the γ_i factors it is convenient to use plasma frequency via

$$\frac{1}{\lambda^2(0)} = \frac{8\pi e^2 N(0) \sum n_i v_i^2}{3c^2} = \frac{\langle \omega_p^2 \rangle}{c^2},$$

so knowing partial ω_{pi}^2 we can express γ_i as

$$\gamma_i = \frac{\omega_{pi}^2}{\sum \omega_{pi}^2}$$

The partial and total plasma frequencies were reported from DFT calculations [22], giving $\gamma_1 = 0.71$ and $\gamma_1 = 0.29$ for a full and for a nodal gap, respectively, and $\gamma_1 = 0.77$ and $\gamma_1 = 0.23$ from de Haas–van Alphen measurements [63]. In the case of specific heat analysis, no Fermi velocities or plasma frequencies are reported and we can only use a pure 2D approximation where $nv^2 = k_F^2/\pi m = k_F^2/\hbar^2\pi^2 N(0)$. Reported densities of states are roughly the same, so the contribution to the superfluid density depends on the Fermi wave vector and is roughly a quarter for the middle band, consistent with the above numbers.

Although the modulation of the gaps might play some role in determining the temperature dependence of the superfluid density, and the gaps must satisfy a self-consistency relation in a multiband system, the largest gap will always have the BCS-like temperature variation. At least in the case of specific heat data analysis, the gaps were calculated self-consistently and they, indeed, confirm the above statement. We therefore can compare two scenarios: one which mimics ARPES and specific heat findings where there are two effective gaps, nodeless and nodal (with different partial densities of states for two different experiments), and the alternative when the gaps possess d-wave character everywhere. The latter must be true for all hole-like sheets of the Fermi surface if the pairing potential changes sign along the diagonals of the Brillouin zone. In that case the normalized superfluid density will be just a simple single-gap d wave.

When analyzing $\rho_s(T)$, we should notice that deviation from d-wave calculations do not leave much room for any full gap contribution to the superfluid density. If it was present, at a level more that 0.1 of the total ρ_s, it would result in significantly exceeding $\rho_s(T)$ over the curve for a d-wave case. Based on this comparison we can disregard any contributions from a full-gap superfluid in both clean $x = 0$ and $x = 0.07$ samples with an accuracy of less than 0.1 of the total superfluid density.

IV. CONCLUSION

Along with the power-law behavior of $\Delta\lambda(T) \sim T^{1.4}$ at low temperatures, the temperature response of the superfluid in both clean and dirty samples is not only consistent with the existence of line nodes in the superconducting gap, but does not leave much room for any contribution from Fermi surfaces with a large and dominant full gap, as suggested by ARPES [32] and heat capacity [33].

In conclusion, our resistivity and TDR London penetration depth studies on high quality pure and isoelectron Na-substituted KFe_2As_2 find behavior which is consistent with the expectations for a superconductor with symmetry-imposed line nodes.

ACKNOWLEDGMENTS

We thank W. E. Straszheim for performing WDS analysis and P. Hirschfeld, A. Chubukov and R. M. Fernandes for useful discussions. This work was supported by the US Department of Energy (DOE), Office of Science, Basic Energy Sciences, Materials Science and Engineering Division. The research was performed at the Ames Laboratory, which is operated for the US DOE by Iowa State University under Contract No. DE-AC02-07CH11358. The single-crystal growth at the University of Tennessee and Rice University was supported by US DOE, BES under Grant No. DE-FG02-05ER4620 (P.D.).

[1] T. Y. Chen, Z. Tesanovic, R. H. Liu, X. H. Chen, and C. L. Chien, Nature (London) **453**, 1224 (2008).
[2] A. D. Christianson, E. A. Goremychkin, R. Osborn, S. Rosenkranz, M. D. Lumsden, C. D. Malliakas, I. S. Todorov, H. Claus, D. Y. Chung, M. G. Kanatzidis *et al.*, Nature (London) **456**, 930 (2008).
[3] I. I. Mazin, D. J. Singh, M. D. Johannes, and M. H. Du, Phys. Rev. Lett. **101**, 057003 (2008).
[4] I. I. Mazin, Nature (London) **464**, 183 (2010).
[5] H. Fukazawa, Y. Yamada, K. Kondo, T. Saito, Y. Kohori, K. Kuga, Y. Matsumoto, S. Nakatsuji, H. Kito, P. M. Shirage *et al.*, J. Phys. Soc. Jpn. **78**, 083712 (2009).
[6] M. Rotter, M. Tegel, and D. Johrendt, Phys. Rev. Lett. **101**, 107006 (2008).
[7] M. Rotter, M. Pangerl, M. Tegel, and D. Johrendt, Angew. Chem. Int. Ed. **47**, 7949 (2008).
[8] M. A. Tanatar, J.-Ph. Reid, H. Shakeripour, X. G. Luo, N. Doiron-Leyraud, N. Ni, S. L. Bud'ko, P. C. Canfield, R. Prozorov, and L. Taillefer, Phys. Rev. Lett. **104**, 067002 (2010).
[9] J.-Ph. Reid, M. A. Tanatar, X. G. Luo, H. Shakeripour, N. Doiron-Leyraud, N. Ni, S. L. Bud'ko, P. C. Canfield, R. Prozorov, and L. Taillefer, Phys. Rev. B **82**, 064501 (2010).

[10] R. T. Gordon, C. Martin, H. Kim, N. Ni, M. A. Tanatar, J. Schmalian, I. I. Mazin, S. L. Bud'ko, P. C. Canfield, and R. Prozorov, Phys. Rev. B **79**, 100506(R) (2009).

[11] R. T. Gordon, H. Kim, N. Salovich, R. W. Giannetta, R. M. Fernandes, V. G. Kogan, T. Prozorov, S. L. Bud'ko, P. C. Canfield, M. A. Tanatar *et al.*, Phys. Rev. B **82**, 054507 (2010).

[12] G. Mu, J. Tang, Y. Tanabe, J. Xu, S. Heguri, and K. Tanigaki, Phys. Rev. B **84**, 054505 (2011).

[13] J. S. Kim, B. D. Faeth, and G. R. Stewart, Phys. Rev. B **86**, 054509 (2012).

[14] J. S. Kim, B. D. Faeth, Y. Wang, P. J. Hirschfeld, G. R. Stewart, K. Gofryk, F. Ronning, A. S. Sefat, K. Y. Choi, and K. H. Kim, Phys. Rev. B **86**, 014513 (2012).

[15] K. Cho, M. A. Tanatar, N. Spyrison, H. Kim, Y. Song, P. Dai, C. L. Zhang, and R. Prozorov, Phys. Rev. B **86**, 020508 (2012).

[16] R. Prozorov, K. Cho, H. Kim, and M. A. Tanatar, J. Phys. Conf. Ser. **449**, 012020 (2013).

[17] J.-Ph. Reid, A. Juneau-Fecteau, R. T. Gordon, S. R. de Cotret, N. Doiron-Leyraud, X. G. Luo, H. Shakeripour, J. Chang, M. A. Tanatar, H. Kim *et al.*, Supercond. Sci. Technol. **25**, 084013 (2012).

[18] R. Thomale, C. Platt, W. Hanke, J. Hu, and B. A. Bernevig, Phys. Rev. Lett. **107**, 117001 (2011).

[19] A. Chubukov, Annu. Rev. Condens. Matter Phys. **3**, 57 (2012).

[20] T. Das, EPJ Web Conf. **23**, 00014 (2012).

[21] A. Glatz and A. E. Koshelev, Phys. Rev. B **82**, 012507 (2010).

[22] K. Hashimoto, A. Serafin, S. Tonegawa, R. Katsumata, R. Okazaki, T. Saito, H. Fukazawa, Y. Kohori, K. Kihou, C. H. Lee *et al.*, Phys. Rev. B **82**, 014526 (2010).

[23] H. Kawano-Furukawa, C. J. Bowell, J. S. White, R. W. Heslop, A. S. Cameron, E. M. Forgan, K. Kihou, C. H. Lee, A. Iyo, H. Eisaki *et al.*, Phys. Rev. B **84**, 024507 (2011).

[24] J. K. Dong, S. Y. Zhou, T. Y. Guan, H. Zhang, Y. F. Dai, X. Qiu, X. F. Wang, Y. He, X. H. Chen, and S. Y. Li, Phys. Rev. Lett. **104**, 087005 (2010).

[25] J.-Ph. Reid, M. A. Tanatar, A. Juneau-Fecteau, R. T. Gordon, S. R. de Cotret, N. Doiron-Leyraud, T. Saito, H. Fukazawa, Y. Kohori, K. Kihou *et al.*, Phys. Rev. Lett. **109**, 087001 (2012).

[26] A. F. Wang, S. Y. Zhou, X. G. Luo, X. C. Hong, Y. J. Yan, J. J. Ying, P. Cheng, G. J. Ye, Z. J. Xiang, S. Y. Li *et al.*, Phys. Rev. B **89**, 064510 (2014).

[27] L. Taillefer, B. Lussier, R. Gagnon, K. Behnia, and H. Aubin, Phys. Rev. Lett. **79**, 483 (1997).

[28] M. Abdel-Hafiez, V. Grinenko, S. Aswartham, I. Morozov, M. Roslova, O. Vakaliuk, S. Johnston, D. V. Efremov, J. van den Brink, H. Rosner *et al.*, Phys. Rev. B **87**, 180507 (2013).

[29] V. Grinenko, D. V. Efremov, S.-L. Drechsler, S. Aswartham, D. Gruner, M. Roslova, I. Morozov, K. Nenkov, S. Wurmehl, A. U. B. Wolter *et al.*, Phys. Rev. B **89**, 060504 (2014).

[30] F. F. Tafti, A. Juneau-Fecteau, M.-E. Delage, S. Rene de Cotret, J.-Ph. Reid, A. F. Wang, X.-G. Luo, X. H. Chen, N. Doiron-Leyraud, and L. Taillefer, Nat. Phys. **9**, 349 (2013).

[31] R. M. Fernandes and A. J. Millis, Phys. Rev. Lett. **111**, 127001 (2013).

[32] K. Okazaki, Y. Ota, Y. Kotani, W. Malaeb, Y. Ishida, T. Shimojima, T. Kiss, S. Watanabe, C.-T. Chen, K. Kihou *et al.*, Science **337**, 1314 (2012).

[33] F. Hardy, A. E. Böhmer, D. Aoki, P. Burger, T. Wolf, P. Schweiss, R. Heid, P. Adelmann, Y. X. Yao, G. Kotliar *et al.*, Phys. Rev. Lett. **111**, 027002 (2013).

[34] S. Kittaka, Y. Aoki, N. Kase, T. Sakakibara, T. Saito, H. Fukazawa, Y. Kohori, K. Kihou, C.-H. Lee, A. Iyo *et al.*, J. Phys. Soc. Jpn. **83**, 013704 (2014).

[35] F. Bouquet, Y. Wang, R. A. Fisher, D. G. Hinks, J. D. Jorgensen, A. Junod, and N. E. Phillips, Europhys. Lett. **56**, 856 (2001).

[36] A. Damascelli, D. H. Lu, K. M. Shen, N. P. Armitage, F. Ronning, D. L. Feng, C. Kim, Z.-X. Shen, T. Kimura, Y. Tokura, Z. Q. Mao, and Y. Maeno, Phys. Rev. Lett. **85**, 5194 (2000).

[37] J. S. Kim, E. G. Kim, G. R. Stewart, X. H. Chen, and X. F. Wang, Phys. Rev. B **83**, 172502 (2011).

[38] V. Grinenko, S.-L. Drechsler, M. Abdel-Hafiez, S. Aswartham, A. U. B. Wolter, S. Wurmehl, C. Hess, K. Nenkov, G. Fuchs, D. V. Efremov, B. Holzapfel, J. van den Brink, and B. Buechner, Phys. Status Solidi B **250**, 593 (2013).

[39] Y. Liu, M. A. Tanatar, V. G. Kogan, H. Kim, T. A. Lograsso, and R. Prozorov, Phys. Rev. B **87**, 134513 (2013).

[40] K. Kihou, T. Saito, S. Ishida, M. Nakajima, Y. Tomioka, H. Fukazawa, Y. Kohori, T. Ito, S.-i. Uchida, A. Iyo *et al.*, J. Phys. Soc. Jpn. **79**, 124713 (2010).

[41] M. A. Tanatar, N. Ni, S. L. Bud'ko, P. C. Canfield, and R. Prozorov, Supercond. Sci. Technol. **23**, 054002 (2010).

[42] M. A. Tanatar, R. Prozorov, N. Ni, S. L. Bud'ko, and P. C. Canfield, US Patent 8,450,246 (1 Sept. 2011).

[43] C. T. Van Degrift, Rev. Sci. Instrum. **46**, 599 (1975).

[44] R. Prozorov and V. G. Kogan, Rep. Prog. Phys. **74**, 124505 (2011).

[45] R. Prozorov, R. W. Giannetta, A. Carrington, and F. M. Araujo-Moreira, Phys. Rev. B **62**, 115 (2000).

[46] W. N. Hardy, D. A. Bonn, D. C. Morgan, R. Liang, and K. Zhang, Phys. Rev. Lett. **70**, 3999 (1993).

[47] H. Kim, M. A. Tanatar, Y. J. Song, Y. S. Kwon, and R. Prozorov, Phys. Rev. B **83**, 100502 (2011).

[48] M. A. Tanatar, N. Ni, C. Martin, R. T. Gordon, H. Kim, V. G. Kogan, G. D. Samolyuk, S. L. Bud'ko, P. C. Canfield, and R. Prozorov, Phys. Rev. B **79**, 094507 (2009).

[49] M. A. Tanatar, N. Ni, A. Thaler, S. L. Bud'ko, P. C. Canfield, and R. Prozorov, Phys. Rev. B **82**, 134528 (2010).

[50] Y. Liu, M. A. Tanatar, W. E. Straszheim, B. Jensen, K. W. Dennis, R. W. McCallum, V. G. Kogan, R. Prozorov, and T. A. Lograsso, Phys. Rev. B **89**, 134504 (2014).

[51] K. Cho, H. Kim, M. A. Tanatar, J. Hu, B. Qian, Z. Q. Mao, and R. Prozorov, Phys. Rev. B **84**, 174502 (2011).

[52] N. W. Salovich, H. Kim, A. K. Ghosh, R. W. Giannetta, W. Kwok, U. Welp, B. Shen, S. Zhu, H.-H. Wen, M. A. Tanatar *et al.*, Phys. Rev. B **87**, 180502 (2013).

[53] P. J. Hirschfeld and N. Goldenfeld, Phys. Rev. B **48**, 4219 (1993).

[54] A. B. Vorontsov, M. G. Vavilov, and A. V. Chubukov, Phys. Rev. B **79**, 140507 (2009).

[55] V. Mishra, G. Boyd, S. Graser, T. Maier, P. J. Hirschfeld, and D. J. Scalapino, Phys. Rev. B **79**, 094512 (2009).

[56] K. Ohishi, Y. Ishii, I. Watanabe, H. Fukazawa, T. Saito, Y. Kohori, K. Kihou, C.-H. Lee, H. Kito, A. Iyo *et al.*, J. Phys. Conf. Ser. **400**, 022087 (2012).

[57] H. Kim, V. G. Kogan, K. Cho, M. A. Tanatar, and R. Prozorov, Phys. Rev. B **87**, 214518 (2013).

[58] G. Li, W. Z. Hu, J. Dong, Z. Li, P. Zheng, G. F. Chen, J. L. Luo, and N. L. Wang, Phys. Rev. Lett. **101**, 107004 (2008).
[59] K. Hashimoto, K. Cho, T. Shibauchi, S. Kasahara, Y. Mizukami, R. Katsumata, Y. Tsuruhara, T. Terashima, H. Ikeda, M. A. Tanatar *et al.*, Science **336**, 1554 (2012).
[60] M. Abdel-Hafiez, S. Aswartham, S. Wurmehl, V. Grinenko, C. Hess, S.-L. Drechsler, S. Johnston, A. U. B. Wolter, B. Büchner, H. Rosner *et al.*, Phys. Rev. B **85**, 134533 (2012).
[61] C. C. Homes, S. V. Dordevic, M. Strongin, D. A. Bonn, R. Liang, W. N. Hardy, S. Komiya, Y. Ando, G. Yu, N. Kaneko *et al.*, Nature (London) **430**, 539 (2004).
[62] V. G. Kogan, Phys. Rev. B **87**, 220507 (2013).
[63] T. Terashima, M. Kimata, N. Kurita, H. Satsukawa, A. Harada, K. Hazama, M. Imai, A. Sato, K. Kihou, C.-H. Lee *et al.*, J. Phys. Soc. Jpn. **79**, 053702 (2010).